Experimental investigation and gyrokinetic simulations of multi-scale electron heat transport in JET, AUG, TCV

A. Mariani,[1,2,*] N. Bonanomi,[3] P. Mantica,[2] C. Angioni,[3] T. Görler,[3] O. Sauter,[4] G.M. Staebler,[5] Eurofusion JET1 contributors,[†] Eurofusion MST1 contributors,[‡] ASDEX Upgrade team,[§] TCV team,[¶] and ITPA transport & confinement group[**]

[1]Department of Physics "G. Occhialini", University of Milano-Bicocca, Milano, Italy
[2]Institute for Plasma Science and Technology, CNR, Milano, Italy
[3]Max-Planck-Institut für Plasmaphysik, Garching, Germany
[4]École Polytechnique Fédérale de Lausanne (EPFL), Swiss Plasma Center (SPC), Lausanne, Switzerland
[5]General Atomics, San Diego, United States of America

(Dated: July 23, 2021)

Tokamaks dominated by electron heating like ITER could possibly suffer from the consequences of an electron temperature gradient (ETG) mode destabilisation, which could develop a turbulent electron heat flux capable of setting an upper limit to the achievable electron temperature peaking, resulting in a degradation of the fusion performance. An effort is carried out in the paper to collect and compare the results of dedicated plasma discharges performed during the last years at three of the major European tokamaks, TCV, AUG and JET, by analysing the electron heat transport for cases presumably compatible with ETGs relevance given the actual theoretical understanding of these instabilities. The response of the electron temperature profiles to electron heat flux changes is experimentally investigated by performing both steady state heat flux scans and perturbative analysis by radio frequency heating modulation. The experimental results are confronted with numerical simulations, ranging from simple linear gyrokinetic or quasi-linear runs, to very computationally expensive nonlinear multi-scale gyrokinetic simulations, resolving ion and electron scales at the same time. The results collected so far tend to confirm the previously emerging picture indicating that cases with a proper balance of electron and ion heating, with similar electron and ion temperatures and sufficiently large electron temperature gradient, could be compatible with a non negligible impact of ETGs on the electron heat transport. The ion heating destabilises ETGs not only by increasing the ion temperature but also thanks to the stabilisation of ion-scale turbulence by a synergy of fast ions and $E \times B$ shearing which are in some cases associated to it. The stabilising effect of plasma impurities on ETGs is still under investigation by means of multi-scale gyrokinetic simulations, and also direct experimental measurements of density and temperature fluctuations at electron scales would be needed to ultimately assess the impact of ETGs.

I. INTRODUCTION

Improving the knowledge of the electron heat transport properties in tokamaks is gaining importance in view of designing new devices like ITER, which will be dominated by electron heating due to electron cyclotron resonance heating (ECH) and alpha heating. Indeed, with the fusion power being proportional to the square of the ion temperature at a given density, the only way to obtain optimal performance in such devices is connected with the capacity of indirectly heating ions by collisional heat exchange from electrons. Therefore, a hypothetical incapacity to heat electrons would result in poor fusion performance. This is directly connected to the concept of 'temperature stiffness', which refers to the degree to which the radial temperature profiles respond to changes in the applied heat fluxes. A 'stiff' electron temperature profile, i.e. a T_e profile which does not peak when increasing the applied electron heat flux $q_{e,ext.}$, due to the development of a turbulent outward radial heat flux which balances $q_{e,ext.}$, could be detrimental to these devices. The study of the generation of a possible strong turbulent electron transport leading to a high electron stiffness, depending on plasma parameters, is thus a key point. In general, the observed levels of turbulent transport in tokamak plasmas, in both the ion and electron channels, are the result of drift-wave micro-instabilities driven by the free energy available in the plasma pressure gradients. In particular, core transport in present tokamaks is currently mostly ascribed to turbulence driven by the nonlinear (NL) saturation of ion-scale micro-instabilities ($k_\theta \rho_i \leq 1$, where k_θ is the poloidal wave number and ρ_i the ion Larmor radius), such as the ion temperature gradient (ITG) modes, which are driven by the logarithmic gradient of the ion temperature $\nabla \ln T_i$, and the trapped electron modes (TEM), driven by both the logarithmic gradients of the electron temperature $\nabla \ln T_e$ and the electron density $\nabla \ln n_e$. In particular, the turbulence generated by the NL saturation of TEM is a source of 'electron temperature stiffness' for sufficiently large values of the TEM drive, resulting in an upper boundary for the normalised T_e logarithmic gradient $R/L_{Te} = -R\nabla T_e \cdot \hat{r}/T_e$, with R the plasma major radius and $\hat{r}$ the radial unit vector. However, it has been shown that electron temperature gradient (ETG) modes

* Electronic address: alberto.mariani@istp.cnr.it
† See the author list of 'Overview of JET results for optimising ITER operation' by J. Mailloux et al to be published in Nuclear Fusion Special issue: Overview and Summary Papers from the 28th Fusion Energy Conference (Nice, France, 10-15 May 2021) for the Eurofusion JET1 conributors.
‡ See Labit et al. 2019 (https://doi.org/10.1088/1741-4326/ab2211) for the Eurofusion MST1 contributors.
§ See Meyer et al. 2019 (https://doi.org/10.1088/1741-4326/ab18b8) for the TCV team.
¶ See Coda et al. 2019 (https://doi.org/10.1088/1741-4326/ab25cb) for the Eurofusion JET1 conributors.
** See https://portal.iter.org/departments/POP/ITPA/TC/Pages/default.aspx for the ITPA transport & confinement group.

[1], which can be destabilized at electron-scales by increasing R/L_{Te}, can also impact the electron heat transport, both by directly producing a turbulent q_e and by exchanging energy with lower-k_θ ITG-TEM turbulence through multi-scale coupling [2–9]. Therefore, the relative role of TEM and ETG in setting an upper boundary for the electron temperature peaking has to be determined depending on plasma parameters. ETGs could play a role in the electron heat transport when mixed ion and electron heating is applied to plasmas. For these cases, a proper balance of ion heating, decreasing the ETG R/L_{Te} linear threshold (proportional to $(1+Z_{\rm eff}T_e/T_i)$[10], where $Z_{\rm eff}$ is the effective charge), and electron heating (pushing R/L_{Te} towards threshold while increasing the threshold due to T_e/T_i increase), could destabilize them, possibly leading to similar R/L_{Te} thresholds for TEM and ETGs. Also all mechanisms that stabilize ITGs, such as $E\times B$ shearing or fast ions (FI) from neutral beam injection (NBI) and/or ion cyclotron resonance heating (ICH), may open a favourable window for ETG destabilization due to multi-scale interactions. Moreover FI can linearly destabilize ETGs due to FI contribution to T_i/T_e. A great effort is actually devoted to analyse different machines, comparing experimental and numerical results, within the framework of EUROfusion and of the ITPA Transport & Confinement group. In this paper, the analysis of plasmas of three different tokamaks, i.e. the Joint European Torus (JET, at Culham, UK), ASDEX Upgrade (AUG, at Garching, DE) and the Tokamak à Configuration Variable (TCV, at Lausanne, CH), is presented. Dedicated plasma discharges have been analysed experimentally and modelled numerically, by means of gyrokinetic (GK) codes (GENE [11, 12] and GKW [13]) and the reduced quasi-linear model TGLF [14]. A detailed review and comparison of these cases at mid-radius, concerning the experimental and numerical analysis of the impact of ETGs on electron heat transport, including the new multi-scale GK analysis of a selected AUG discharge, is the focus of this paper.

II. EXPERIMENTAL ANALYSIS

An overview of the experiments that have been performed at the three tokamaks, as well as the corresponding experimental analysis at mid-radius ($\rho_{tor}=0.5$), follow.

A. Overview of the experiments at TCV, AUG and JET

TCV: two dedicated L-mode discharges, with vacuum magnetic field on the magnetic axis $B_0=1.41T$ and plasma current $I_p=170kA$ have been performed in TCV with a different proportion of deposited ECH ($\sim 0.4-0.7MW$) power on- vs off-axis to perform a heat flux scan. Each pulse presented different phases corresponding to a different proportion of NBI($\sim 1MW$)/ECH power to vary T_e/T_i, with ECH both steady and modulated to allow a perturbative analysis. The TCV results that we include in this paper are published in [5]. **AUG:** Similar experiments have been carried out in AUG [6, 15], producing H-mode discharges with $B_0=2.6T$, $I_p=0.8MA$, injecting $2.5MW$ of ECH (steady and modulated) and $5MW$ of NBI in order to have $T_e\sim T_i$, varying the ECH radial deposition (heat flux scan). **JET:** Following early results pointing to an important role of ETGs in JET [4], very recently dedicated sessions on ETGs have also been performed at JET. Both L- and H-mode plasmas have been obtained, with $B_0=3.3T$, $I_p=2MA$, injecting $0-20MW$ of NBI and up to $6MW$ of ICH (H minority with $n_H/n_e\sim 6\%$, to mainly heat electrons), achieving heat flux scans for a range of T_e/T_i values. The main JET results that we included in our comparison are accepted for publication [16].

B. Experimental results at mid-radius

The response of the T_e profiles to the applied heating can be experimentally investigated by performing normalized electron heat flux scans and/or radio frequency (RF) power modulation analysis. The two methods can be used in conjunction to extract information on the dependence of the gyro-Bohm (gB) normalized electron heat flux $q_{e,gB}$ on R/L_{Te}, yielding experimental values for the threshold $R/L_{Te,crit.}$ for the onset of turbulent transport and for the 'electron stiffness' $\partial q_{e,gB}/\partial R/L_{Te}$. Here the heat flux in gB units is defined as $q_{j,gB}=q_j(e^2R^2B_0^2/\sqrt{m_i}n_eT_e^{5/2})$, where $j=e,i$ indicate electrons or ions, q_j is the radial heat flux per unit surface, e the electron charge, m_i the ion mass. An impact of ETGs on the achievable T_e peaking could be spotted by directly inspecting the heat flux scans, since it would be accompanied by a steep increase of $q_{e,gB}$ with increasing R/L_{Te}. This increase, steeper than the corresponding TEM slope, is here refereed to as 'ETG wall', since it would resemble a wall in the $q_{e,gB}$ vs R/L_{Te} plot.

Steady state heat flux scans have been obtained for TCV, AUG and JET, corresponding to the experiments that have been summarized in the introduction. RF (ECH) modulation measurements have been obtained for TCV and AUG (for JET the use of ICH H minority heating prevented the use of ICH modulation due to too broad deposition profiles and too long FI slowing down times). The results at $\rho_{tor}=0.5$ are shown in Fig.1 (a)-(c) for the three machines.

Variations of turbulence relevant parameters like R/L_{ne}, R/L_{Ti}, T_e/T_i, $Z_{\rm eff}$, q (safety factor) and $\hat{s}$ (magnetic shear), between pulses, are unavoidable during real experiments. Therefore, it is not possible tu perform 'ideal' steady state electron heat flux scans, where only R/L_{Te} is varied. Details on the variation of parameters different form R/L_{Te} in the electron heat flux scans for TCV, AUG and JET are given in [5], [15] and [16]. However, such variations are very small when comparing cases with ECH deposition on-axis versus mixed on- and off-axis, while they can become moderate only if comparing extreme cases with ECH deposition on-axis versus off-axis.

For TCV, the comparison of points with on- vs off-axis ECH indicates moderate stiffness for both ECH only (red) and mixed NBI-ECH case (black). Only the perturbative analysis allows to measure an ETG-compatible local stiffness for the mixed NBI-ECH point ($T_e\sim T_i$) with ECH on-axis (ma-

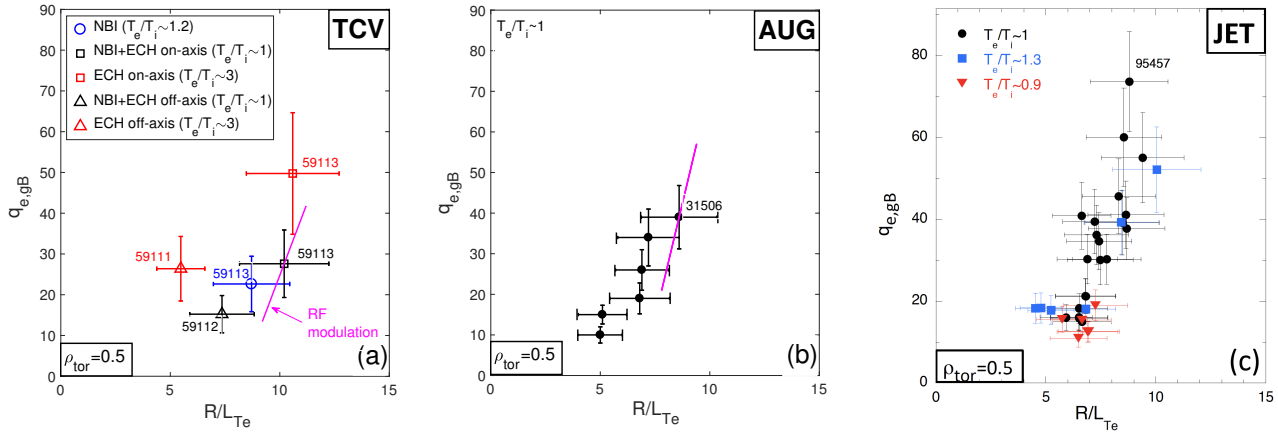

Figure 1. Experimental electron heat flux scans at mid-radius $\rho_{tor} = 0.5$ for TCV (a), AUG (b) and JET (c). The electron heat flux in gB units $q_{e,gB}$ is shown versus R/L_{Te}. After [5] (a), [6, 15] (b), [16] (c).

genta line), which becomes the best candidate to show an ETG contribution to q_e. More in detail, by the perturbative analysis of the heat wave propagation due to RF modulated ECH, for the mixed NBI-ECH cases the TEM and ETG thresholds have been found similar, resulting in a mixed continuous TEM/ETG branch with a stiffness resulting from the combination of the two branches. A much larger ETG/TEM proportion was needed to match the ECH RF data for the mixed NBI/ECH case with ECH deposition on-axis, resulting in a much larger local stiffness, compatible with a large role of ETGs. An independent estimate of the stiffness was obtained by studying the propagation of a sawtooth magnetohydrodynamic mode, which was found to pollute the T_e modulation measurements, for that case, with results that are in very good agreement with the ECH modulation analysis. Due to this agreement, the local slope that has been obtained with ST analysis is shown in Fig.1 (a) by a magenta line and it is generically referred to as 'RF modulation'. Further details can be found in [5].

All the experimental points of the AUG heat flux scan with $T_e \sim T_i$ are shown in Fig.1 (b). Similarly to TCV, the steady state scan trend is compatible with TEM stiffness. However, the local slope has been evaluated using RF modulation for pulse #31506 (largest $q_{e,gB}$) and it is compatible with ETG presence. Unfortunately, for both TCV and AUG there is a lack of higher $q_{e,gB}$ points which could show the actual presence of an ETG wall.

For JET (Fig.1 (c)), the $T_e/T_i = 0.9$ high-pedestal H-modes (red) are stuck to low $q_{e,gB}$ due to gB normalisation (high T_e), while the $T_e/T_i = 1.3$ L-modes (blue) present a mild TEM-consistent stiffness. Thus only the $T_e \sim T_i$ low-pedestal H-modes and L-modes (black) are compatible with a possible ETG wall due to the highest $q_{e,gB}$ pulse #95457. Despite the JET scan with $T_e \sim T_i$ is compatible with an 'ETG wall' picture, it lacks RF modulation data to compare with.

Comparing the three tokamaks, hence confirms that the best candidates to show a possible ETG role in producing q_e are the ones with a balance of ion and electron heating, leading to a concomitance of $T_e \sim T_i$ and large R/L_{Te}.

III. LINEAR MULTI-SCALE GYROKINETIC RESULTS

Linear multi-scale simulations at $\rho_{tor} = 0.5$ have been performed in order to characterise the turbulence regime using the GENE code for a selection of TCV, AUG and JET cases. The pulses with $T_e \sim T_i$ and large R/L_{Te} have been identified in Section II B to be the best candidates to show an ETG impact to q_e. In particular, among them, the ones with the largest $q_{e,gB}$ have been identified for AUG (#31506, H-mode) and JET (#95457, L-mode) to be the most promising to possibly show a role for ETGs, given the results of the RF modulation analysis (AUG) and due to the fact that the JET pulse #95457 could be placed on an ETG wall (after an inspection of the points in Fig.1 (c) with $T_e \sim T_i$ and largest $q_{e,gB}$, that show a large slope). The same holds for the TCV case with ECH deposition on-axis and NBI injection (selected phase from #59113 pulse, L-mode, balck point on the right in Fig.1 (a)), for which the perturbative analysis indicates an ETG-compatible local stiffness. These three cases are thus selected for TCV, AUG and JET to perform the gyrokinetic analysis. The case with ECH deposition on-axis but without NBI and the case with only NBI are also considered for TCV for comparison (other two phases from #59113, red point on the right and blue point in Fig.1 (a)).

GENE solves the GK equations coupled with the Maxwell equations within a δf approximation, using a set of field-aligned coordinates $\{x, y, z, v_\parallel, \mu\}$ in the reduced 5-dimensional GK phase space. x, y and z are the radial, binormal and parallel (to B) coordinates in configuration space, while $v_\parallel$ and μ are the parallel velocity and the magnetic moment. The simulations are carried out in the flux-tube limit using realistic geometries, reconstructed using numerical equilibria from CHEASE [17] (TCV) and EFIT [18] (AUG, JET), taking into account collisions (using a Landau-Boltzmann collisional op-

	TCV ECH (59113)	TCV ECH+NBI (59113)	TCV NBI (59113)	AUG (31506)	JET (95457)
T_e/T_i	3.04	∼1	1.16	∼1	∼1
Z_{eff}	2.50	2.80	2.80	1.4	1.5
R/L_{Te}	10.59	10.20	8.71	8	9
R/L_{Ti}	5.94	5.55	15.07	6.5	4.59
R/L_{ne}	3.69	4.85	6.07	0.91	3.12
q	1.65	1.34	1.42	2.07	1.82
$\hat{s}$	0.99	1.19	1.14	6.85	1.05
κ	1.17	1.12	1.13	1.32	1.28
δ	0.1	0.08	0.09	0.05	0.05
β_e $[10^{-3}]$	2.01	2.37	1.54	5	1.12
ν_c $[10^{-3}]$	0.91	1.33	1.77	1.87	0.57
γ_E $[c_s/R]$	∼0	0.14	0.34	0.04	∼0

Table I. Main plasma parameters for the analyzed pulses at ρ_{tor} = 0.5.

erator) and finite-β (electromagnetic) effects (considering only $B_\perp$ fluctuations), kinetic ions and electrons, kinetic impurity species when considered, kinetic FI when considered. Rotation effects such as $E \times B$ shear and parallel flow shear are taken into account for the TCV cases when NBI are injected. Detailed linear multi-scale and nonlinear ion-scale convergence tests have been performed for the numbers of grid points $[n_{kx}, n_{ky}, n_z, n_{v\parallel}, n_\mu]$ and for the x and y box sizes L_x and L_y. Nonlinear multi-scale convergence tests were not accessible due to limited computational resources.

The main plasma parameters of the selected cases are listed in Table I.

Here, in particular, κ indicates the elongation, δ the triangularity and $\beta_e = 2\mu_0 n_e T_e/B_0$ is the ratio of the electron plasma pressure to the magnetic pressure, with μ_0 the vacuum permeability. The GENE collisional parameter $\nu_c = 2.3031 \times 10^{-5} \ln\Lambda\ R[m] n_e[10^{19} m^{-3}]/T_e[keV]^2$ ($\ln\Lambda = 24 - \ln(\sqrt{10^{13} n_e[10^{19} m^{-3}]}/10^3 T_e[keV])$ the Coulomb logarithm) is listed instead of the electron-ion thermal collision rate $\nu_{ei} = 4(n_i/n_e)\sqrt{T_e/m_e}\nu_c/R$, since ν_c only depends on the measured quantities n_e and T_e while ν_{ei} changes given the number of considered species (n_i adapted invoking neutrality). The impurities which cause Z_{eff} in the three tokamaks are C (TCV), B and W (AUG) and Be, C, Ne, Ni and W (JET). For the JET case, for consistency with the NL multi-scale GK simulation, where it was impossible to include three kinetic impurities for lack of computational resources, impurities are taken into account in the simulations using a single C species, to reproduce the experimental Z_{eff} and ion dilution without increasing the cost of the simulations. Given the experimental concentrations a main ion dilution resulting in a main ion concentration of $n_i/n_e \sim 0.883$ is found. This is compatible with considering 2.0% of Be and 0.045% of a second impurity with Z=25 (a mix of W and Ni). The use of 2 impurities is too expensive in a multiscale simulations so we decided to concentrate the effect of the plasma impurities (effect on the ETG linear threshold, on the ITG linear drive though main ion dilution and on ITG non-linear stiffness) in one single species using carbon. This choice was made as using C it was possible to reproduce in a very good way both the main ion dilution and the Z_{eff} with one single impurity. Using 1.7% of C we have $n_i/n_e \sim 0.898$ and $Z_{\text{eff}} = 1.51 \sim 1.5$. In this way the effect of the main ion dilution is taken into account in the simulations as well as the effect of Z_{eff} within a $\lesssim 2\%$ error bar without increasing the cost of the simulations. A similar procedure, lumping the impurities in single C impurity resulting in $n_i/n_e = 0.92$ (keeping $Z_{\text{eff}} \sim 1.4$), has been applied to AUG when impurities are taken into account. Finally, $\gamma_E = -(x/q)(\partial\Omega_{tor}/\partial x)R/c_s$ is the $E \times B$ shearing rate, where Ω_{tor} is the toroidal angular velocity and $c_s = \sqrt{T_e/m_i}$ the ion sound speed. The parallel flow shear γ_p was computed, when γ_E was taken into account (TCV cases with NBI), consistently with the pure toroidal flow assumption [$\gamma_p \simeq (q/\epsilon)\gamma_E$, where ϵ is the inverse aspect ratio at mid-radius]. It has to be pointed out that kinetic FI coming from NBI are retained in TCV simulations ($n_{FI}/n_e \sim 10\%$, $T_{FI}/T_e \sim 16$, $R/L_{n,FI} \sim 14$, $R/L_{T,FI} \sim 2$ at $\rho_{tor} = 0.5$), while they are neglected for AUG ($n_{FI}/n_e \sim 1\%$: NBI) and JET ($n_{FI}/n_e \sim 0.2\%$: NBI and ICH), since their density fraction is much lower than for TCV.

All the cases are found to be ITG-dominant at ion-scales except for those from TCV when ECH is injected, which are TEM-dominant. ETGs are found unstable at electron scales. The impact of ETGs on q_e can be roughly predicted using a simple criterion, which states that ETGs should contribute to q_e if the peak of the ratio γ/k_y of the growth rate of the most unstable mode and the corresponding poloidal wavenumber is larger at electron-scales than at ion-scales [19, 20]. γ/k_y is shown versus k_y for TCV, AUG and JET cases in Fig.2 (a), (b) and (c) respectively.

For AUG, the lower $R/L_{Ti} = 3.65$ value has been considered together with the experimental one ($R/L_{Ti} = 6.5$), consistently with the NL multi-scale analysis. Indeed, despite being below the experimental error bar, this value is chosen for the NL multi-scale simulations (see Sec.V). This R/L_{Ti} is obtained by matching q_i with ion-scale NL simulations (see Sec. IV), neglecting the effects of fast ions, rotation and impurities, as it is done in the multi-scale runs due to computational constraints. Neglecting these effects leads to an increase of the ion stiffness, and a lower value of R/L_{Ti} is needed to match the ion heat flux with respect to the experimental one. For JET, instead of the experimental $R/L_{Ti} = 4.59$, the two values $R/L_{Ti} = 5.17, 5.77$ are considered. They allow to match the experimental q_i at the two ends of its error bar with ion-scale NL GK simulations (see Sec.IV), testing the sensitivity to R/L_{Ti} (NL GK multi-scale simulations have been run with both the R/L_{Ti} values for JET, see Sec.V). For TCV the ETG-relevance criterion is only met for the mixed NBI-ECH case, as expected. In particular, the condition is fulfilled because of a strong linear stabilisation of ion-scale TEMs by NBI FI. For AUG, the criterion is always met. In particular, the ion-scales are strongly suppressed at the lower value of R/L_{Ti}, indicating a possible strong role of ETGs for that case. Similar simulations have been run with GKW for AUG, and the results are published in [6] (see Fig.19), indicating a role for ETGs for $R/L_{Te} \geq 6$ at experimental R/L_{Ti}. The AUG runs just give a lower boundary for the ETG R/L_{Te} threshold, since they set

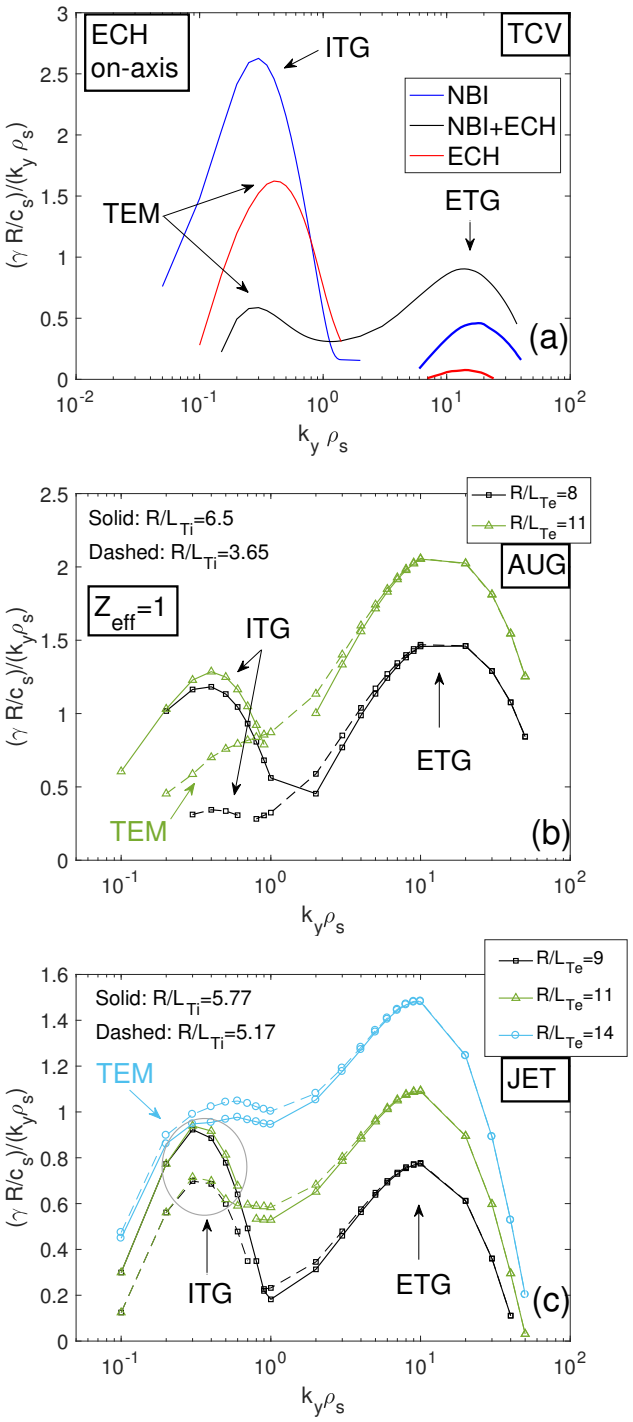

Figure 2. Linear GENE scans of γ/k_y, normalised with $\rho_s c_s/R$ ($\rho_s = c_s/\Omega_i$ is the ion Larmor radius, where ω_i is the ion cyclotron frequency) for the selected TCV (a), AUG (b) and JET (c) cases. The TCV parameters are taken from pulse 59113, while for JET they are consistent with pulse 95467. After [5] (a), [16] (c)

$Z_{\text{eff}} = 1 < 1.4 = Z_{\text{eff,exp.}}$, thus already under-predicting the linear threshold by $\sim 20\%$. $Z_{\text{eff}} = 1$ is kept for AUG consistently in linear, NL ion-scale and NL multi-scale runs, since it was impossible to use the exp. value of Z_{eff} in the NL multi-scale runs due to insufficient computational resources. However, the impact of impurities has also been evaluated for AUG, by means of linear GK simulations (see the following paragraph) and using a faster quasi-linear model (see Sec. VI). JET results predict a non-negligible contribution of ETGs to q_e for $R/L_{Te} \geq 11$ when $R/L_{Ti} = 5.77$ and for $R/L_{Te} \geq 9$ when $R/L_{Ti} = 5.17$.

In order to investigate the Z_{eff} dependence of the R/L_{Te} threshold for an impact of ETGs on q_e, linear scans of γ/k_y vs R/L_{Te} have been performed for selected k_y values considering the AUG and JET cases, comparing the results obtained by taking into account the impurities (with experimental Z_{eff}) with the ones coming from simulations where the impurities are neglected ($Z_{\text{eff}} = 1$). To further test the sensitivity of the results to R/L_{Ti}, it has been varied consistently with Fig.2 (b) and (c), i.e. considering the two values $R/L_{Ti} = 3.65, 6.5$ for AUG and the two values $R/L_{Ti} = 5.17, 5.77$ for JET. The results are shown in Fig.3. Here, following [6] (see Fig.20), for each considered case (four cases obtained by separately varying the considered machine and R/L_{Ti}) two sets of k_y are compared: the first around the γ/k_y maximum at ion scales (black squares: $Z_{\text{eff}} = 1$; blue triangles: $Z_{\text{eff}} = Z_{\text{eff,exp.}}$), the second around the γ/k_y ETG maximum at electron scales (red squares: $Z_{\text{eff}} = 1$; magenta triangles: $Z_{\text{eff}} = Z_{\text{eff,exp.}}$). The plots on the left indicate AUG results, while the plots on the right indicate JET ones. Moreover, the first row corresponds to the largest R/L_{Ti}, while the second row corresponds to the smallest R/L_{Ti}. The ETG relevance criterion is met when R/L_{Te} is sufficiently large so that at least one k_y value from the electron-scale set corresponds to a γ/k_y that is larger than all the γ/k_y values corresponding to the ion-scale set of wavenumbers. This is equivalent to stating that the ETG relevance criterion is met for $R/L_{Te} > R/L_{Te,crit.}$, where $R/L_{Te,crit.}$ can be directly visualised looking at the figure, as the R/L_{Te} so that the upper end of the electron-scale 'stripe' (k_y values corresponding to ETGs) crosses the upper end of the ion-scale 'stripe'. From an inspection of the results, it follows that $R/L_{Te,crit.}$ increases with increasing Z_{eff}, consistently with linear physics (ETG linear threshold $R/L_{Te,linear} \propto 1+Z_{\text{eff}}T_e/T_i$). However, $R/L_{Te,crit.}$ should not be confused with the ETG linear threshold, since it gives a measure of the threshold for ETGs to nonlinearly contribute to q_e, which is different (larger) from the threshold for ETGs to be linearly destabilised ($R/L_{Te,crit.} > R/L_{Te,linear}$). The impact of Z_{eff} is small-moderate [$\Delta(R/L_{Te,crit.}) = R/L_{Te,crit.}(Z_{\text{eff}} = Z_{\text{eff,exp.}}) - R/L_{Te,crit.}(Z_{\text{eff}} = 1) \sim 1$] for the larger R/L_{Ti} cases ((a) and (b)), while it is small [$\Delta(R/L_{Te,crit.}) < 0.5$] for the smaller R/L_{Ti} cases ((c) and (d)). It has also to be noted that impurities, for similar Z_{eff}, are more effective at stabilising ion scales for the JET case.

More details on part of the simulations that are shown in this section can be found in [5], [6], [16], corresponding to TCV, AUG and JET cases, respectively. This also holds for the TCV results of Sec. VI and the JET results of Sections IV and VI. Regarding AUG, part of the GENE linear GK results and all the NL multi-scale GK results are published here for the first time.

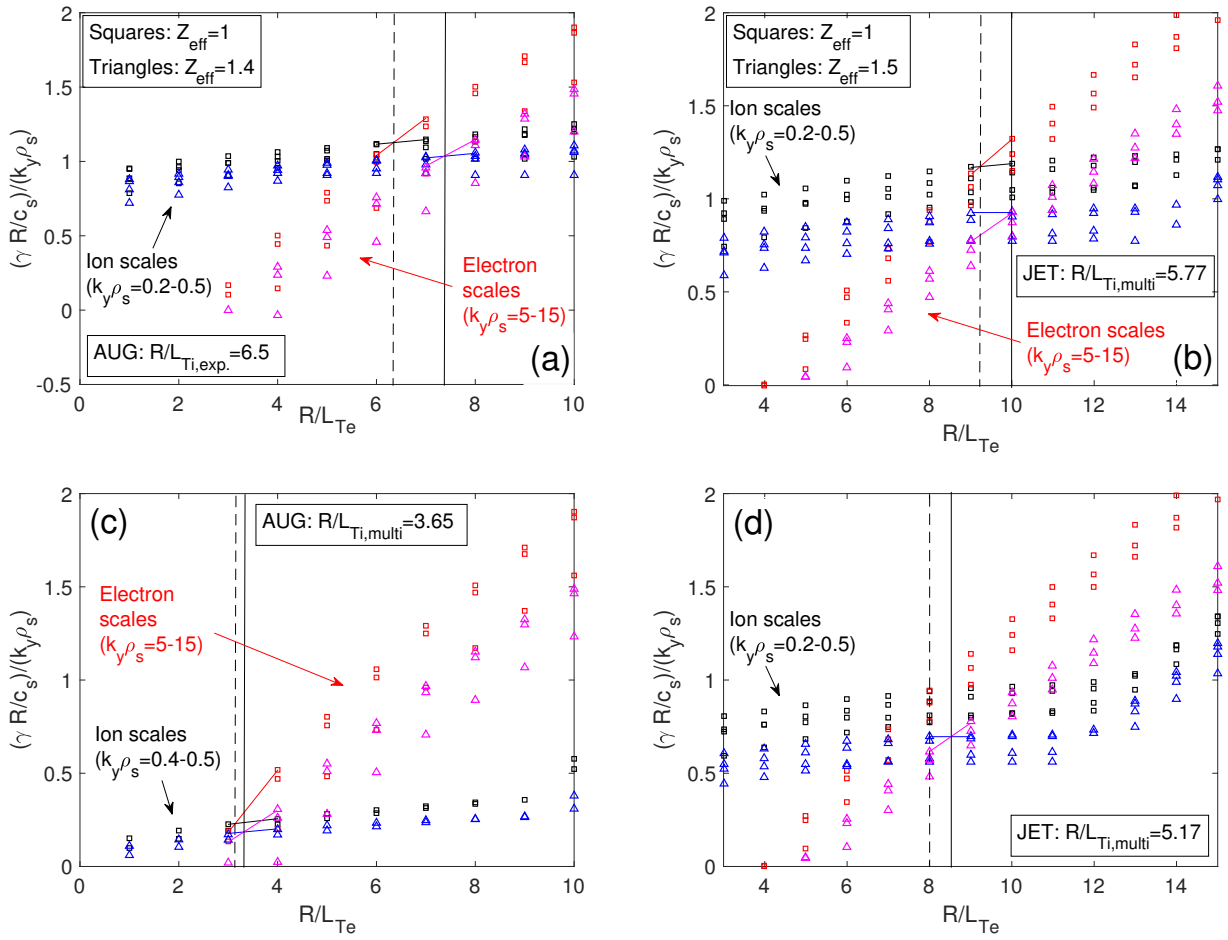

Figure 3. Effect of $Z_{\rm eff}$ on ETG impact: GENE linear γ/k_y ratio vs R/L_{Te} for JET (left) and AUG (right) cases, for selected k_y intervals corresponding to ion scale (black/blue) and electron scale (red/magenta) γ/k_y peaks. Two values of R/L_{Ti} are considered for each case (different rows), as well as two values of $Z_{\rm eff}$ ($Z_{\rm eff}$ = 1: squares, reference $Z_{\rm eff}$: triangles). The dashed and solid vertical lines indicate the R/L_{Te} corresponding to the crossing of electron-scale and ion-scale γ/k_y stripes, for $Z_{\rm eff}$ = 1 and reference $Z_{\rm eff}$ respectively.

IV. NON-LINEAR ION-SCALE GYROKINETIC RESULTS

GENE NL ion-scale simulations have been performed to interpret the experimental results, in order: 1) to test if the GK flux levels match the experimental ones, or a contribution from ETGs (lacking in ion-scale runs) is needed; 2) to compare the GK stiffness with the experimental one, evidencing a possible ETG role if the experimental stiffness is underpredicted by ion-scale GK. Both electron and ion heat channels are investigated for AUG and JET, where the ion-scale is ITG-dominant and very sensitive to R/L_{Ti}, while only the electron channel is investigated for TCV where TEMs are dominant at ion-scales. Indeed, by looking at the ion channel for TCV cases with ECH, it is found that q_i is much lower than q_e, with similar error bars. Considering for example the mixed ECH/NBI case with ECH deposition on-axis, which is the best candidate to possibly show an ETG role, one has $q_{e,exp.}/q_{i,exp.} \sim 5$. The GENE predictions for the absolute value of fluxes fall lower than experiment, but the ratio $q_{e,GENE}/q_{i,GENE} \sim 4$ is not far from the experiment. It could be possible by increasing R/L_{Ti} within error bars to have a better match of q_i, and go nearer to the experimental q_e with ion-scale fluxes, although the ITG contribution to q_e in this TEM dominant case is small. However, this contribution to q_e would be only a bias but it would not significantly change the electron stiffness (i.e. the slope of $q_{e,gB}$ vs R/L_{Te}). Conversely, considering the multi-scale nonlinear dynamics, by increasing R/L_{Ti}, the ITGs would be destabilised, with a resulting ETG stabilisation due to ITG zonal flows. This would go in the opposite direction with respect to trying to explain the experimental results, since it would be even more in disagreement with the RF modulation prediction of an high local electron stiffness for that case. The simulations cover ion scales up to $k_y\rho_s = 3.2, 2.4, 1.8$ for TCV, AUG and JET, respectively. The following grids are used in the GK reduced 5-dimensional phase space: $[n_{kx}, n_{ky}, n_z, n_{v\|}, n_\mu]$ = [256, 64, 32, 64, 16], [256, 32, 32, 32, 12] and [256, 24, 32, 32, 12] for TCV, AUG and JET, respectively.

The TCV GK results are shown by black and red diamonds in Fig.4 (a), corresponding to ECH only and mixed ECH-NBI

cases, respectively.

Two GK simulations have been performed for each experimental case: the first with experimental parameters and the second by reducing R/L_{Te} from $\sim$ 10 to 7, to evaluate the stiffness. The experimental points with ECH off-axis (lower R/L_{Te}) have been kept in the figure to give an idea of the experimental stiffness. However, the GK runs have been done with parameters from the cases with ECH on-axis (pulse #59113), therefore GK and experimental stiffness should be only qualitatively compared. The results indicate that GK explains both the flux levels and the stiffness for the ECH only case, while for the mixed ECH-NBI case GK both strongly under-predicts the flux levels and the stiffness, invoking the ETGs as a possible player to fill those gaps. In particular, a synergic interplay of stabilizing effects of fast ions and $E \times B$ shearing ($\gamma_E \sim 0.14$), both due to NBI injection, is observed for this case, reducing the TEM-driven $q_{e,gB}$ to negligible values compared to the experimental ones. This effect has been observed by repeating the reference ion-scale NL GK simulation for this case, first removing the $E \times B$ shear, then the FI and finally both of them. It is found that the stabilising effect of $E \times B$ shearing is larger when FI are accounted for (see figure 15 (b) in [5]). Two NL runs have been performed for the AUG case, varying $R/L_{Te} = 8, 11$. They are indicated by blue diamonds in Fig.4 (b). The experimental points of the R/L_{Te} scan with $T_e \sim T_i$ have all been kept in the figure (black dots with error bars) in order to give an idea of the experimental local stiffness, while the GK simulations have been run with the parameters from pulse #31506. The logarithmic gradient of T_i has been set to $R/L_{Ti} = 3.65 < 6.5 = R/L_{Ti,exp.}$ in order to match the experimental value of $q_{i,gB}$ with GK (see the smaller picture in Fig. 3 (b)). This is needed since the T_i profile is very stiff with respect to q_i variations, due to ITG-dominant ion scales. Moreover, impurities and $E \times B$ shear ($\gamma_E \sim 0.04$) have been neglected, to better compare with the multi-scale runs (see Sec. V). For the same reason, FI have not been included ($n_{FI}/n_e \sim 1\%$, $T_{FI}/T_e \sim 15$, $R/L_{n,FI} \sim 6$, $R/L_{T,FI} \sim 2$). However, since for this case the FI density fraction is 10 times smaller than the TCV ECH+NBI case and the γ_E is 3.5 times smaller, one should expect a significantly smaller impact of FI and $E \times B$ shear on NL fluxes than for TCV. The results of the simulations show that even if for the AUG case the experimental $q_{e,gB} = 39$ is only moderately under-predicted by GK ($q_{e,gB} = 27.4$, slightly below the $\pm 20\%$ error bar), the experimental stiffness (from RF modulation: magenta line) is strongly under-predicted. Turning to JET results (Fig.4 (c) and (d), corresponding to the electron and ion channels, respectively), Three R/L_{Ti} were considered in the GK runs ($R/L_{Ti} = 4.8, 5.77, 6$: red, blue and magenta, respectively) and scans in R/L_{Te} were performed for each value of R/L_{Ti}. Only the experimental points of the R/L_{Te} scan with $T_e \sim T_i$ have all been kept in the figure in order to give an idea of the experimental local stiffness, while the GK simulations have been run with the parameters from pulse #95467. FI have been neglected for consistency with the multi-scale runs similarly to AUG (FI density fraction is 50 times smaller for JET than for the TCV ECH+NBI case). As visible in Fig.4 (d), the ion heat flux is very stiff in R/L_{Ti}, due to ITGs. Changing R/L_{Ti} also impacts q_e, which increases by $\sim 100\%$ when changing R/L_{Ti} from 4.88 to 6. However, changing R/L_{Ti} does not impact the R/L_{Te} stiffness of q_e. For $R/L_{Ti} = 5.77$, a study of the effect of R/L_{ne} was also performed, increasing the nominal value by 40%. When increasing R/L_{ne}, $q_{e,gB}$ increases by about 40% due to stronger TEMs, while q_i decreases, without changing the R/L_{Te} stiffness of q_e. Summarizing these JET results, while the single experimental point can be reproduced by varying the input parameters within error bars in GK simulations, the experimental slope of $q_{e,gB}$ vs R/L_{Te} is underestimated by ion-scale GK. A mechanism providing a q_e contribution scaling with R/L_{Te} would be needed, which could come from ETGs.

V. NON-LINEAR MULTI-SCALE GYROKINETIC RESULTS

Collecting the results from the three tokamaks, it seems that for the cases with $T_e \sim T_i$ the ion-scales are not sufficient to explain the experimental flux levels and/or the T_e stiffness. As a consequence, dedicated multi-scale NL GENE runs have been performed to quantify the contribution of ETGs to both q_e and to its slope vs R/L_{Te}, for AUG and JET. This has not yet been done for TCV, since the priority has been given to larger tokamaks where $\rho^* = \rho_i/a$ effects (called 'global' effects, where ρ_i is the ion Larmor radius and a the plasma minor radius), which are not retained in the GENE flux-tube version, should not play a role. Actually, a global multi-scale NL GK simulation would require more than our available computational resources. For AUG, the same parameters of the ion-scale runs (thus with $Z_{\text{eff}} = 1$), have been kept.

To reduce the computational cost of these heavy runs, the same strategy has been adopted for the AUG and JET cases with the lowest value of R/L_{Te}: first an ion-scale simulation has been run, keeping the same number of k_x modes that is needed for the corresponding multi-scale. Then, after the NL convergence of the fluxes, a checkpoint has been saved and the simulation has been re-started from it expanding the k_y grid to include electron scales. This procedure helps avoiding (or at least reducing) the initial overshoot, with corresponding substantial temporary reduction of the nonlinear time step (during the overshoot), saving computational time. Then, the simulations with larger R/L_{Te} have been run starting from checkpoints of the runs with lower R/L_{Te}, by changing only R/L_{Te}. For each R/L_{Te} a $\Delta t \sim 25 - 35\ R/c_s$ and $\Delta t \sim 40 - 50\ R/c_s$ statistics has been collected for the AUG and JET cases, corresponding to 1-2 or 2-3 'large' flux oscillations, respectively. Each multi-scale run used $\sim 8 - 12$ Million CPU hours on the A3 partition of MARCONI-CINECA supercomputer.

For AUG, two multi-scale runs have been performed, for $R/L_{Te} = 8, 11$. In particular, the simulation with experimental $R/L_{Te} = 8$ has been initially run including only the ion scales and has been prolonged expanding the k_y grid ($n_{ky} = 32 \rightarrow 512$) to include electron scales, as explained above. The radial and binormal box sizes for AUG are $[L_x, L_y] = [118.2, 83.8]\rho_s$, corresponding to $k_{y,min}\rho_s = (2\pi/L_y)\rho_s = 0.075$, $k_{x,min}\rho_s = (2\pi/L_x)\rho_s = 0.053$. The simulations have

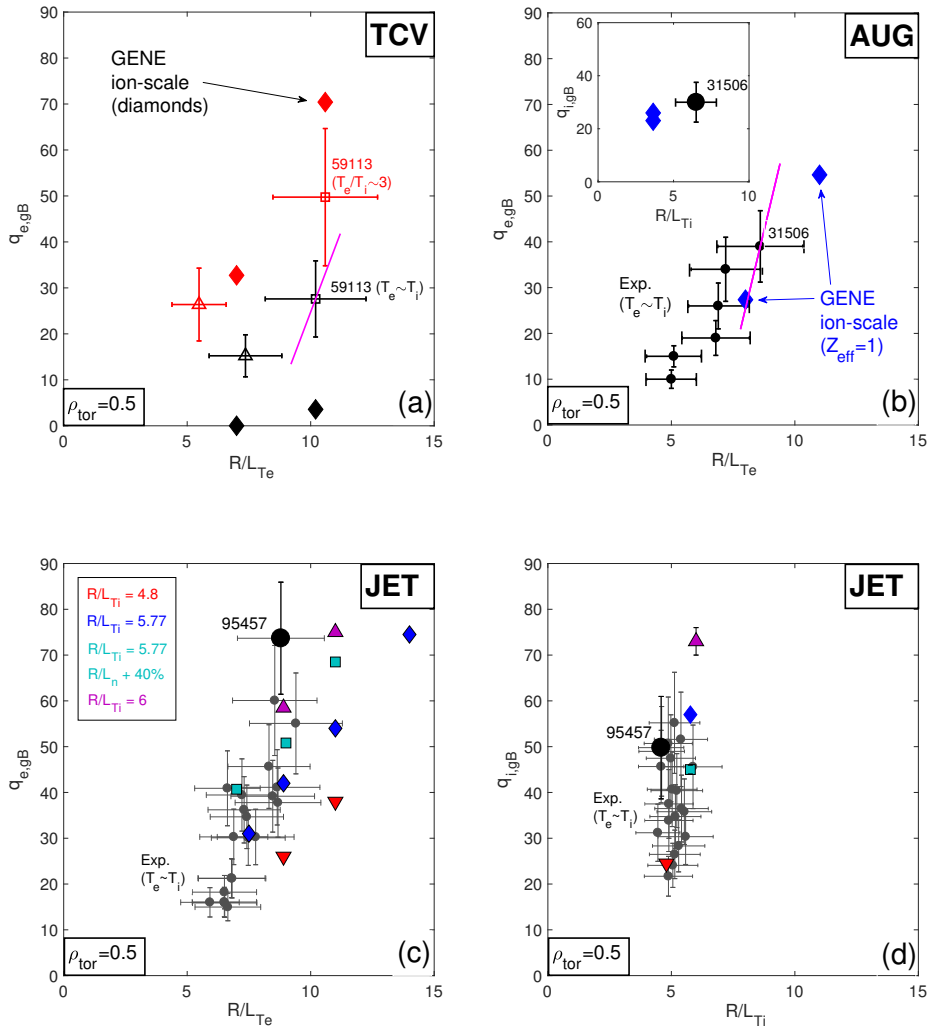

Figure 4. GENE NL ion-scale $q_{e,gB}$ vs R/L_{Te}, compared with the exp. results of Fig.1, for TCV (a), AUG (b) and JET (c). GENE NL ion-scale $q_{i,gB}$ vs R/L_{Ti} is indicated for AUG in the small box in (b), while it is shown in (d) for JET. The TCV case with NBI only is not shown as well as the JET exp. cases with $T_e \neq T_i$. After [5] (a), [6, 15] (b), [16](c)/(d).

been run with $[n_{kx}, n_{ky}, n_z, n_{v\parallel}, n_\mu] = [1280, 512, 32, 32, 12]$ grid points. Due to the constraints on computational resources, this was the highest resolution possible for this study (the same holds for the JET simulations that will be shown in the following), but the effect of these resolutions could potentially be important and could be explored in the future. The results of the AUG multi-scale simulations (stars) are compared with the ion-scale fluxes (diamonds) in Fig.5 (a).

The corresponding q_e spectra are presented in Fig.6 (a).

The impact of ETGs, coming from electron scales ($k_y\rho_s > 1$), on q_e, increases with increasing R/L_{Te}. It is moderate/large ($\sim$ 33%) at experimental $R/L_{Te} = 8$, while it becomes large ($\sim$ 55%) at $R/L_{Te} = 11$. The multi-scale stiffness in particular is well aligned with the RF modulation result (magenta). The observed moderate/large impact of ETGs for AUG case is thus in line with the linear prediction of ETGs impacting q_e for $R/L_{Te} > 6$, being both the considered R/L_{Te} values beyond 6.

Following the same strategy, three multi-scale runs have been performed for the JET case for $R/L_{Te} = 9, 11, 14$, with $R/L_{Ti} = 5.77$. For the JET case, impurities have been accounted for, the same way as in ion-scale NL and linear runs. The x and y box sizes have been set to $[L_x, L_y] = [88.6, 83.8]\rho_s$, corresponding to $k_{y,min}\rho_s = (2\pi/L_y)\rho_s = 0.075 \sim k_{x,min}\rho_s = (2\pi/L_x)\rho_s = 0.071$, and $[n_{kx}, n_{ky}, n_z, n_{v\parallel}, n_\mu] = [1536, 512, 32, 32, 12]$ grid points have been used. The results, shown in Fig.5 (b)/(c) (blue stars) and Fig.6 (b), indicate a negligible ($\sim$ 5%) impact of ETGs on q_e at experimental $R/L_{Te} = 9$, increasing with R/L_{Te} but remaining moderate ($\sim$ 18%) at $R/L_{Te} = 14$, in line with the linear prediction of an ETG impact for $R/L_{Te} > 11$ when $R/L_{Ti} = 5.77$. The stiffness of the multi-scale fluxes still does not explain the experimental slope.

Following the analysis of Figs.2 and 3, that indicates a larger role for ETGs at smaller R/L_{Ti} based on the γ/k_y crite-

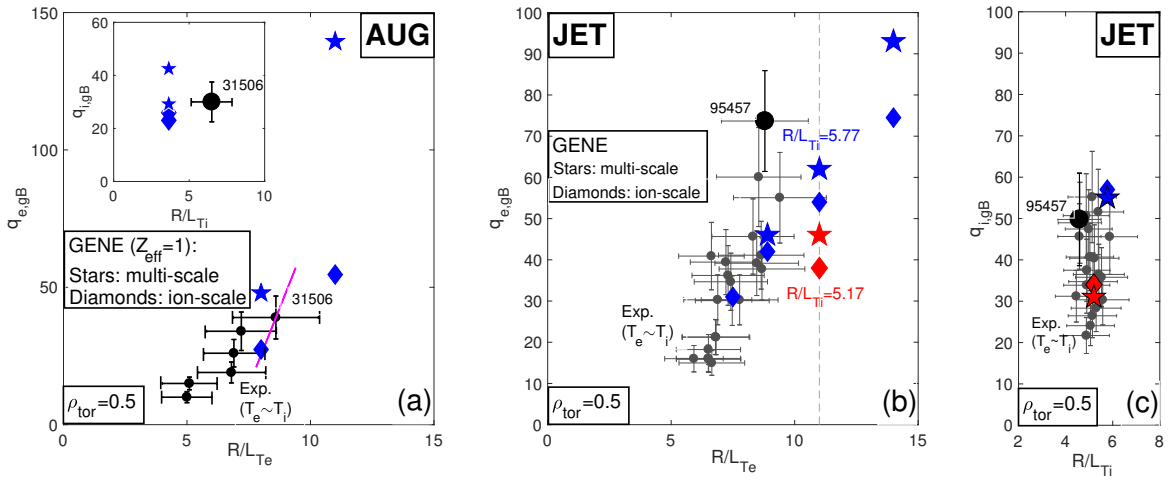

Figure 5. Multi-scale GENE electron heat flux in gB units $q_{e,gB}$ vs R/L_{Te} (stars), compared with the corresponding ion-scale fluxes (diamonds), for AUG (a) and JET (b). For JET, the two values $R/L_{Ti} = 5.17$ (red) and $R/L_{Ti} = 5.77$ (blue) are considered, which allow to match the experimental q_i at the two extremes of its error bar with ion-scale NL runs. Corresponding ion heat flux in gB units $q_{i,gB}$ vs R/L_{Ti} in (a) (small box) and (c). After [16] (b)-(c).

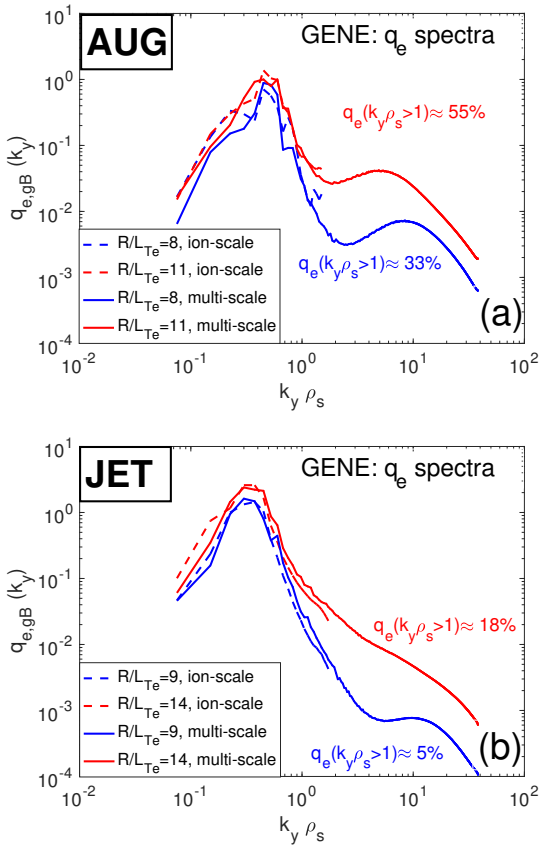

Figure 6. Electron heat flux spectra in gB units $q_{e,gB}(k_y)$, satisfying $q_{e,gB} = \sum_{k_y} q_{e,gB}(k_y)$, corresponding to the multiscale simulations of AUG (a) and JET (b) with extreme values of R/L_{Te}, i.e. $R/L_{Te} = 8, 11$ for AUG and $R/L_{Te} = 9, 14$ for JET. After [16].

rion introduced in Section III, an additional multi-scale simulation has been run for the intermediate $R/L_{Te} = 11$ setting the lower $R/L_{Ti} = 5.17$ value that allows to match q_i at the lower boundary of its experimental error bar with ion-scale NL runs. This is done to check if indeed a larger impact of ETGs on q_e is observed in the multi-scale simulation by decreasing R/L_{Ti}, and if it could help to get closer to the experimental electron heat flux level. The fluxes are shown in red in Fig.5 (b) (electron channel) and (c) (ion channel). The corresponding q_e spectra are shown in Fig.7.

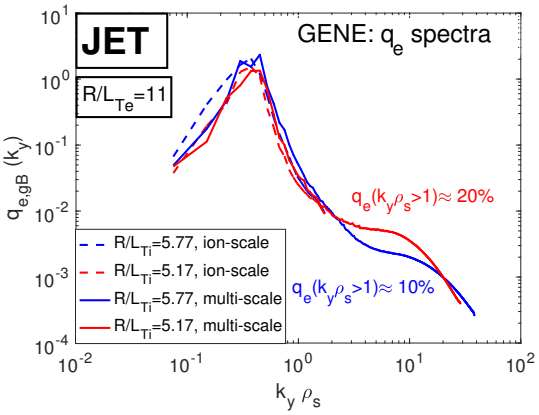

Figure 7. Electron heat flux spectra in gB units $q_{e,gB}(k_y)$, corresponding to the simulations at $R/L_{Te} = 11$, comparing the runs with $R/L_{Ti} = 5.17, 5.77$ following the same color code of Fig.5 (b)/(c). After [16].

The results indicate that despite the ETG fraction is increasing with decreasing R/L_{Ti}, the decrease of the q_e fraction coming from ion-scales is larger, so that the overall q_e is smaller for $R/L_{Ti} = 5.17$ than for $R/L_{Ti} = 5.77$. The

comparison of the q_e spectra corresponding to $R/L_{Ti} = 5.77$ (blue) and $R/L_{Ti} = 5.17$ (red) in Fig.7, in particular, indicates that ETGs contribution to q_e increases only by 10% with decreasing R/L_{Ti}, going from 10% for $R/L_{Ti} = 5.77$ to 20% for $R/L_{Ti} = 5.17$. Summarising the JET multi-scale GK results, it is not possible to match both experimental values of q_e and q_i by first matching q_i within its experimental error bar with ion-scale simulations and then performing multi-scale runs to re-compute q_e and q_i. It could still be possible that some cross-scale effect like the one observed in [2, 3, 7], consisting in a backward effect of ETGs on ion scales when ion scales are marginally stable, could allow to match both the electron and ion heat fluxes with multi-scale simulations further lowering R/L_{Ti} closer to the ITG threshold. However, the very high ion stiffness of the experimental points seems to indicate that this last picture should not be likely for the considered JET case, since the cross-scale effect observed in [2, 3, 7] should imply a reduction of the ion stiffness. Moreover, for this 'high ion stiffness' case, the search of an 'optimal' value of R/L_{Ti} close to the ITG threshold to observe such cross-scale effect would require a fine R/L_{Ti} scan of such very heavy GK NL multi-scale simulations, which is beyond both the scope of this work and the available computational resources.

Summing up, a significant impact of ETGs on q_e is observed in AUG GK NL multi-scale simulations, where it is possible to match both the experimental q_e flux level and the stiffness (from perturbative analysis) with GK, while for JET a small role is observed for ETGs and it is not possible to match both the q_e flux level and the experimental stiffness (from the steady state heat flux scan). The main difference in the simulation settings between AUG and JET is the fact that the impurities have been neglected for AUG, while they have been retained for JET. As a consequence the impact of the ETGs on q_e is expected to be overestimated for AUG by GK. An analysis of the impact of impurities on the results, made with the computationally cheaper quasilinear model TGLF, is presented in the following section. Moreover, it has to be noted that effects coming from both FI and rotation shear have been neglected for both AUG and JET, due to limited resources. Anyway, since these effects are expected to be larger for AUG ($\gamma_E \sim 0$ for JET and n_{FI}/n_e is 5 times larger for AUG wrt. JET), they could lead to a stabilisation of ion scales (with a possible synergic effect of FI and rotation shear as for TCV), letting ETGs further grow for AUG, even increasing the discrepancy between AUG and JET. Unlike the FI and the rotation shear, electromagnetic effects and collisionality have been taken into account in the simulations. Both effects are expected to be larger for AUG than for JET (β_e is ~ 4.5 tmes larger for AUG, ν_c is ~ 3.3 times larger for AUG), and they could act stabilising ion scales, therefore letting ETGs develop. This could help further explaining the discrepancy between AUG and JET multi-scale results. Further details about such possible effect from collisions on subdominant TEMs for the AUG case can be found in [15]. Finally, cross-scale effects due to marginally unstable ITGs like those in [2, 3, 7], which are not showing up in our JET simulations, could possibly help explaining the lack of ETGs in our JET runs, but finding the conditions for these effects to manifest is beyond our possibilities at present time.

VI. MULTI-SCALE TGLF STAND-ALONE RESULTS

R/L_{Te} scans have been performed with the stand-alone version of TGLF for AUG and JET starting from reference parameters (Table I). The two most recent versions of TGLF have been used: TGLF SAT1-geo (11/2019: improved description of geometrical effects and calibration against GK with respect to SAT1 [14]) and SAT2 [21]. These scans have been run with the aim of further evaluating the impact of the impurities on the results. Comparing the two TGLF runs for AUG (blue and green in Fig.8 (a) for $Z_{\rm eff} = 1$ and $= 1.4$ respectively), the effect of impurities on the ETG wall is not negligible, but however TGLF with both $Z_{\rm eff} = 1$ and $= 1.4$ agrees with the experimental flux within the R/L_{Te} error bar and agrees with both the experimental stiffness (RF modulation: magenta) and the GENE multi-scale stiffness (red stars).

The situation is different for JET (Fig.8 (b)). The stiffness of SAT1-geo in the TEM part of the curve is a bit lower than in experiment and in GENE, but overall acceptable, whilst that of SAT2 is significantly underestimated. Both models feature an ETG wall at quite large values of R/L_{Te}, so that they miss reproducing the experimental uppermost points by a factor > 2 in $q_{e,gB}$, as for the GENE multi-scale, which however does not feature an ETG wall. As a matter of fact, the only case where the TGLF SAT1-geo curve approaches the experimental data also in the uppermost region is that with $Z_{\rm eff} = 1$, which however is experimentally unrealistic. One should note that for JET, since TGLF $q_{i,gB}$ is significantly underestimated at the nominal R/L_{Ti}, also cases with increased R/L_{Ti} (to match $q_{i,gB}$) are shown, which is key for a correct reproduction of multi-scale interactions.

It has to be pointed out that for both AUG and JET cases the impact of $Z_{\rm eff}$ on the up-shift of the 'ETG wall' is larger than what one would expect looking at the results of Fig.3, based on the simple γ/k_y criterion for ETG impact on fluxes.

Due to the strong sensitivity of the TGLF simulations to $Z_{\rm eff}$ for the JET case, and due to the lack of GK multi-scale simulations with impurities to compare with, a more detailed study of the effect of impurities for this case has been pursued in [16], performing TGLF scans of $q_{e,gB}$ vs R/L_{Te}, and considering the real impurity mix: Be, C, Ne, Ni and W, also separating light and heavy impurities. It results that TGLF gets closer to the experimental data, almost explaining them, only when the heavy impurities are neglected. This remains to be understood, with new multi-scale GK runs when resources will be available, where light and heavy impurities are treated separately, and not lumped together in a single C effective impurity as in the multi-scale GK runs presented in Sect.V.

VII. CONCLUSIONS

A collection and comparison of similar experiments that have been performed at the three tokamaks TCV, AUG and JET, assessing the impact of ETG modes on the electron heat

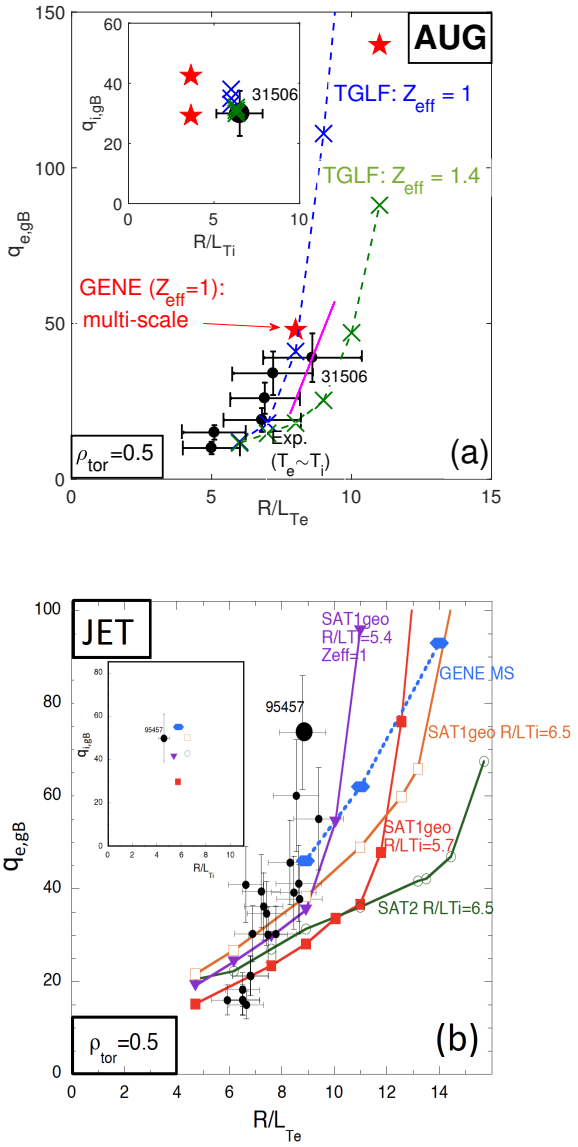

Figure 8. TGLF stand-alone fluxes, compared with exp. points and GENE multi-scale fluxes, for AUG (a) and JET (b). After [16] (b)

transport, is presented in this paper. The experimental observations, coming from dedicated plasma pulses, are interpreted with the help of numerical simulations, including very computationally heavy nonlinear multi-scale gyrokinetic runs. The same experimental framework has been applied to the different machines, consisting in performing steady state electron heat flux scans ($q_{e,gB}$ vs R/L_{Te}), obtained varying the electron heating radial deposition. This is done to study the electron temperature stiffness and test the possible presence of an ETG wall, also varying the ion/electron heating power ratio since it impacts the ETG linear threshold. When available (TCV and AUG), these data are confronted with a perturbative analysis based on ECH radio-frequency modulation or on the study of the propagation of the sawtooth instability, which allows an independent determination of the stiffness. In the following we summarize the main message that can be extracted from this comparison work, with reference to the sections where they are discussed.

Experimental analysis (section II):

- Steady state electron heat flux scan: **TCV and AUG:** TEM-compatible moderate stiffness for all the considered cases; **JET:** TEM-compatible stiffness for most of the considered cases, except for the ones with the largest values of $q_{e,gB}$ and $T_e \sim T_i$, which could possibly indicate the presence of an ETG wall;
- Perturbative analysis (ECH power radio-frequency modulation or sawtooth propagation analysis): **TCV and AUG:** High ETG-compatible stiffness for the cases with $T_e \sim T_i$ and largest R/L_{Te} (corresponding to largest $q_{e,gB}$). **JET:** the perturbative experiment was not performed.
- Comment on the results: in the three tokamaks the resulting experimental picture is that ETGs could possibly impact q_e for cases with $T_e \sim T_i$ and sufficiently high R/L_{Te}, obtained by a conjunction of electron and ion heating, which is in line with the actual theoretical understanding of ETGs.

Experimental data are confronted with linear, nonlinear ion-scale and multi-scale (only AUG, JET) gyrokinetic simulations with the GENE code. The simulations are carried out in the flux-tube limit using realistic geometries, taking into account collisions, electromagnetic effects (only $B_\perp$), kinetic impurities (except for most of the AUG simulations for consistency with the AUG multi-scale where impurities have been neglected due to lack of computational resources), kinetic fast ions and rotation effects ($E \times B$ shear and parallel flow shear) only for TCV cases with NBI.

Linear multi-scale gyrokinetic simulations (section III):

- Three pulses with $T_e \sim T_i$ and large R/L_{Te} are identified to perform the gyrokinetic analysis for TCV, AUG and JET respectively, being the best candidates to possibly show an impact of ETGs on electron heat transport based on the experimental analysis. Two additional cases are considered for TCV for comparison;
- Turbulence regime, ion scales: **TCV:** TEM-dominant (except for NBI-only case, which is ITG-dominant); **AUG and JET:** ITG-dominant;
- Turbulence regime, electron scales: ETG-dominant for all the three machines;
- ETG impact on q_e, based on a simple γ/k_y criterion (ETGs matter if γ/k_y is larger at electron scales than at ion scales): **TCV:** the criterion is only met for the mixed NBI-ECH case with ECH on-axis (due to the strong stabilisation of TEMs by NBI fast-ions); **AUG** (with $Z_{\text{eff}} = 1$): the criterion is met at experimental R/L_{Ti} but an even stronger role is predicted for ETGs at the

lower R/L_{Ti} value that is chosen for the NL multi-scale runs, based on matching q_i with NL ion-scale simulations; **JET:** the criterion is met for $R/L_{Te} > 11$ when $R/L_{Ti} = 5.77$ is chosen to match the experimental q_i at the upper end of its error bar, and for $R/L_{Te} > 9$ when $R/L_{Ti} = 5.17$ is chosen to match the experimental q_i at the lower end of its error bar (both R/L_{Ti} values are considered in the NL multi-scale runs); **comment on the results:** the results confirm that the already mentioned experimental cases with $T_e \sim T_i$ and high R/L_{Te} are good candidates to possibly show an ETGs role. The effect of the fast ions which are produced by the NBI, stabilizing the TEM-dominant ion scales, plays an important role for the TEM-dominant reference TCV case, while for the ITG-dominant AUG and JET cases a larger role is predicted for ETGs when R/L_{Ti} is decreased, consistently with an expected reduced ITG NL zonal flow damping of ETGs;

- Effect of the impurities on the R/L_{Te} threshold for ETG importance based on γ/k_y criterion (tested for AUG and JET, comparing the $Z_{\rm eff} = 1$ case with experimental $Z_{\rm eff}$, also varying R/L_{Ti}): the impact of ETGs on q_e is larger for $Z_{\rm eff} = 1$ than for $Z_{\rm eff} > 1$. The impact of $Z_{\rm eff}$ is small-moderate for the larger R/L_{Ti} cases, while it is small for the smaller R/L_{Ti} cases. Moreover impurities, for similar $Z_{\rm eff}$, are more effective at stabilising ion scales for the JET case compared with the AUG one.

Nonlinear ion-scale gyrokinetic simulations (section IV):

- **TCV:** ECH only case: both flux levels and stiffness are explained by ion-scale runs; mixed NBI-ECH case: both the q_e flux levels and the corresponding stiffness from ECH modulation are strongly under-estimated by ion-scale gyrokinetic results (a synergic effect of fast ions and rotation shear stabilises the ion scales);

- **AUG** (with $Z_{\rm eff} = 1$): The experimental $q_{e,gB}$ is slightly underpredicted by the ion-scale runs, but the stiffness from the perturbative analysis is strongly underpredicted;

- **JET:** The ions are very stiff, therefore changing R/L_{Ti} also strongly impacts q_e. However, varying R/L_{Ti} does not impact the electron stiffness (similar varying R/L_{ne}). As a consequence for JET it is possible to match the experimental $q_{e,gB}$ but not the electron stiffness with ion-scale runs;

- Comment on the results: for some cases it is possible to match the experimental flux levels with ion-scale runs varying the parameters within error bars, but it is not possible to explain the electron stiffness for all the TCV, AUG and JET cases of interest.

Nonlinear multi-scale gyrokinetic simulations (section V):

- Only the AUG and JET cases are considered, since for TCV possible global effects need to be modelled with a global multi-scale simulation with fast ions and $E \times B$ shearing, which is not computationally feasible);

- **AUG** (with $Z_{\rm eff} = 1$): the multi-scale results allow to explain both the experimental flux levels and stiffness as possibly coming from ETGs, and the stiffness that is obtained connecting multi-scale GK results is in good agreement with the result from perturbative analysis (caveat: the impurities have been neglected in the GK runs);

- **JET:** $R/L_{Ti} = 5.77$: the GK fluxes do not explain both the experimental flux levels and stiffness, with ETGs that are found to play a minor role for this case. $R/L_{Ti} = 5.17$: the experimental $q_{e,gB}$ is still underpredicted (it is even smaller than for the corresponding simulation with larger $R/L_{Ti} = 5.77$, due to the reduced contribution of ITG-dominant ion scales);

- Comment to the results: main difference in the GK NL multi-scale simulation settings between AUG and JET: the impurities have been neglected for AUG, while they have been retained for JET, therefore the impact of the ETGs on q_e is expected to be overestimated by GK for AUG; The effects of FI and rotation shear are neglected for both AUG and JET, and they are expected to be larger for AUG: keeping them would probably result in more ETGs for AUG, increasing the disagreement between AUG and JET GK results; electromagnetic effects (from $B_\perp$) and collisions are retained for both AUG and JET, and their impact is expected to be larger for AUG: their effect should increase the ETGs impact, helping explaining the AUG-JET GK disagreement. Finally, a possible alternative explanation for the minor role that is predicted for ETGs for the JET case by the multi-scale runs could come from cross-scale effects like those observed in [2, 3, 7], but they seem incompatible with the observed high experimental ion stiffness.

TGLF stand-alone simulations (section VI):

- Since due to a lack of computational resources it was not possible to investigate in detail the effect of the impurities on the results, repeating the heavy multi-scale runs adding them for AUG or removing them for JET, a quasi-linear analysis has been performed using the stand-alone version of TGLF.

- **AUG:** the effect of impurities is not negligible but it is possible to explain the experimental data with or without adding them, within experimental error bars;

- **JET:** it is possible to get close to explain the experimental data with TGLF only neglecting heavy impurities, that have a large impact on the position of the ETG wall in the $q_{e,gB}$ vs R/L_{Te} plane.

To further test the role of ETGs, sensitivity scans in the multi-dimensional parameter space should be performed with NL multi-scale GK simulations (presently not possible due to their computational cost). This could also help understanding the sensitivity of the results to parameters that are different

from R/L_{Te} and cannot be exactly kept fixed within the experimental steady state electron heat flux scans, as was pointed out in section II. Moreover, density and possibly temperature fluctuations should be experimentally measured at electron scales, and compared with synthetic diagnostics applied to multi-scale GK runs. More conclusive results on the impact of impurities on ETGs are needed, in particular by performing more multi-scale GK simulations with impurity species, possibly separating the effects of light and heavy impurities. This could be useful in turn to better calibrate quasi-linear models like TGLF vs GK and improve the reliability of plasma profiles prediction in cases that are compatible with ETG relevance. Finally, more studies about the impact of electromagnetic effects and rotation shear on ETGs should be performed.

ACKNOWLEDGEMENTS

This work has been carried out within the framework of the EUROfusion Consortium and has received funding from the Euratom research and training programme 2014-2018 and 2019-2020 under grant agreement number 633053. The views and opinions expressed herein do not necessarily reflect those of the European Commission. O. Sauter was supported in part by the Swiss National Foundation. We acknowledge the CINECA award under the ISCRA initiative, for the availability of high performance computing resources and support. Part of the simulations presented in this work were performed at the COBRA HPC system at the Max Planck Computing and Data Facility (MPCDF), Germany. This work was also conducted under the auspices of the ITPA Topical Group on Transport & Confinement. Fig.1 (a), Fig.2 (a) and Fig.4 (a) are adapted, with permission, from [5].

REFERENCES

[1] Dorland W., Jenko F., Kotschenreuther M., and Rogers B.N., 2000 *Phys. Rev. Lett.* **85** 5579
[2] Howard N.T., Holland C., White A.E., Greenwald M., and Candy J., 2014 *Phys. Plasmas* **21** 112510
[3] Howard N.T., Holland C., White A.E., Greenwald M. and Candy J., 2016 *Nucl. Fusion* **56** 014004
[4] Bonanomi N., Mantica P., Citrin J., Goerler T., Teaca B., and JET Contributors, 2018 *Nucl. Fusion* **58** 124003
[5] Mariani A., Mantica P., Brunner S., Fontana M., Karpushov A., Marini C., Porte L., Sauter O., the TCV Team and the EUROfusion MST1 Team, 2019 *Nucl. Fusion* **59** 126017
[6] Ryter F., Angioni C., Dunne M., Fischer R., Kurzan B., Lebschy A., McDermott R.M., Suttrop W., Tardini G., Viezzer E., 2019 *Nucl. Fusion* **59** 096052
[7] Maeyama S., Idomura Y., Watanabe T.-H., Nakata M., Yagi M., Miyato N., Ishizawa A., and Nunami M., Phys. Rev. Lett. 114 (2015) 255002
[8] Marinoni A., Pinsker R.I., Porkolab M., Rost J.C., Davis E.M., Burrell K.H., Candy J., Staebler G.M., Grierson B.A., McKee G.R., 2017 *Nucl. Fusion* **57** 126014
[9] Holland C., Howard N.T. and Grierson B.A., 2017 *Nucl. Fusion* **57** 066043
[10] Jenko F., Dorland W., and Hammett G.W., 2001 *Phys. Plasmas* **8** 4096
[11] Jenko F., Dorland W., Kotschenreuther M., and Rogers B.N., 2000 *Phys. Plasmas* **7** 1904
[12] Görler T., Lapillonne X., Brunner S., Dannert T., Jenko F., Merz F., and Told. D., 2011 *J. Comput. Phys.* **230** 7053
[13] Peeters A.G., Camenen Y., Casson F.J., Hornsby W.A., Snodin A.P., Strintzi D., Szepesi G., 2009 *Comput. Phys. Commun.* **180** 2650
[14] Staebler G.M., Candy J., Howard N.T., and Holland C., 2016 *Phys. Plasmas* **23** 062518
[15] Bonanomi N. *et al.*, to be submitted
[16] Mantica P. *et al.*, accepted for publication by *Nucl. Fusion*
[17] Lütjens H., Bondeson A., Sauter O., 1996 *Comput. Phys. Commun.* **97** 219
[18] Brix M., Hawkes N.C., Boboc A., Drozdov V., Sharapov S.E., and JET-EFDA Contributors, 2008 *Rev. Sci. Instrum.* **79** 10F325
[19] Staebler G.M., Howard N.T., Candy J., and Holland C., 2017 *Nucl. Fusion* **57** 066046
[20] Creely A.J., Rodriguez-Fernandez P., Conway G.D., Freethy S.J., Howard N.T., White A.E. and the ASDEX Upgrade Team, 2019 *Plasma Phys. Control. Fusion* **61** 085022
[21] Staebler G.M., Candy J., Belli E.A., Kinsey J.E., Bonanomi N., and Patel B., 2021 *Plasma Phys. Control. Fusion* **63** 015013